

Dalton Transactions

Accepted Manuscript



This is an *Accepted Manuscript*, which has been through the Royal Society of Chemistry peer review process and has been accepted for publication.

Accepted Manuscripts are published online shortly after acceptance, before technical editing, formatting and proof reading. Using this free service, authors can make their results available to the community, in citable form, before we publish the edited article. We will replace this *Accepted Manuscript* with the edited and formatted *Advance Article* as soon as it is available.

You can find more information about *Accepted Manuscripts* in the [Information for Authors](#).

Please note that technical editing may introduce minor changes to the text and/or graphics, which may alter content. The journal's standard [Terms & Conditions](#) and the [Ethical guidelines](#) still apply. In no event shall the Royal Society of Chemistry be held responsible for any errors or omissions in this *Accepted Manuscript* or any consequences arising from the use of any information it contains.

Thermal structural characterization of the acentric layered perovskite $\text{LiHSrTa}_2\text{O}_7$: X-ray and neutron diffraction, SHG and Raman experiments

Cyrille Galven^a, Denis Mounier^{a,b}, Thierry Pagnier^{c,d}, Emmanuelle Suard^e

Françoise Le Berre^a and Marie-Pierre Crosnier-Lopez^a

^aLUNAM Université du Maine, Institut des Molécules et Matériaux du Mans (IMMM), UMR CNRS 6283, Avenue O. Messiaen, 72085 Le Mans cedex 9, FRANCE

^bEcole Nationale Supérieure du Mans (ENSIM), Université du Maine, Avenue O. Messiaen, 72085 Le Mans cedex 9, FRANCE

^cUniv. Grenoble Alpes, LEPMI, F-38000 Grenoble, France

^dCNRS, LEPMI, F-38000 Grenoble, France

^eInstitut Laüe-Langevin, 6 rue G. Horowitz, 38042 Grenoble Cedex 9, France

Abstract

The present work concerns the thermal structural characterization of the acentric Ruddlesden-Popper $\text{LiHSrTa}_2\text{O}_7$. A previous study, performed with powder neutron diffraction data, has revealed that at room temperature, $\text{LiHSrTa}_2\text{O}_7$ crystallizes in the $Ama2$ space group and that the acentric character is mainly due to the unequal distribution of the Li^+ and H^+ cations on their sites. In this new paper, the thermal behaviour has been studied by several techniques: powder X-ray and neutron diffraction, SHG experiments and Raman spectroscopy. All of them have revealed that $\text{LiHSrTa}_2\text{O}_7$ undergoes a reversible structural transition from an orthorhombic to a tetragonal symmetry around 200°C . This transition is associated to the progressive vanishing of the TaO_6 octahedra tilting, becoming completely straight on in the high temperature form (S.G. $I4/mmm$), and to a variation of the Li^+ and H^+ distribution in the interlayer spacing.

Keywords : layered perovskite, Ruddlesden-Popper, X-ray and neutron diffraction, Raman, ionic exchange, acentric, SHG.

1. Introduction

Among the extensive family of the perovskite phases, the layered Ruddlesden-Popper (RP) compounds^{1,2} form an important groups due to the interesting properties they exhibit. Indeed, some of them are good candidates for ionic exchange or intercalation leading to the formation of numerous new compounds.^{3,10} In addition, we also find RP phases presenting ionic

conductivity^{11,12}, photocatalytic water splitting^{13,17} and exfoliation^{18,19} of the protonated forms. The structure of these layered perovskites, corresponding to the general formula $A'_2[A_{n-1}B_nO_{3n+1}]$, is constituted by BO_6 octahedra connected by corners forming thus blocks of n layers. The A cations are located inside these blocks in the perovskite cages and in a twelve coordination while the A' cations occupied the interlayer spacing between two consecutive blocks. Most often in RP structures, the BO_6 octahedra are slightly tilted inside the perovskite block. Unfortunately, in case of powder samples, these tilts are generally invisible to X-ray diffraction as this technique is not very sensitive to oxygen atoms. That's why, the neutrons diffraction is essential for the structural determination of these oxides due to its better sensitivity to light atoms.

In 2009, we published a complete structural study of the RP phase $Li_2SrTa_2O_7$ ($n = 2$) performed from X-ray and neutron diffraction and completed by Raman experiments.²⁰ We showed that this compound undergoes a structural transition around 230°C due to a progressive vanishing of the TaO_6 octahedra tilting under heating. This work was completed by a second paper concerning the Li^+/H^+ exchange which allows to obtain $LiHSrTa_2O_7$ by a topotactic mechanism.²¹ This new RP phase was characterized at room temperature by neutrons diffraction experiment which revealed its acentric structure since it crystallizes in the $Ama2$ space group (SG). This acentric character was moreover confirmed by a positive second harmonic generation (SHG) response. We also showed that, in spite of the existence of the three RP compounds, $Li_2SrTa_2O_7$, $LiHSrTa_2O_7$ and $H_2SrTa_2O_7$,²² no continuous solid solution $Li_{2-x}H_xSrTa_2O_7$ exists. In order to complete this work on $LiHSrTa_2O_7$, we present in this paper a study concerning its structural behavior in temperature. This work was performed by X-ray and neutron diffraction, second harmonic generation test, DSC and Raman experiments. For neutron diffraction measurements, deuterium was used instead of hydrogen in order to reduce the background and to increase the contrast between D and Li.

2. Experimental

2.1. Synthesis

$LiHSrTa_2O_7$ ($LiDSrTa_2O_7$) was prepared by a Li^+/H^+ (Li^+/D^+) exchange reaction from the mother phase $Li_2SrTa_2O_7$ obtained in powder form by solid state reaction in air as described in reference 20. The ionic Li^+/H^+ exchange is performed with NH_4Cl (Scharlau 99.5%) for $LiHSrTa_2O_7$ or ND_4Cl (Euriso-top 98%) for $LiDSrTa_2O_7$. For both compounds, $Li_2SrTa_2O_7$ is mixed with a large excess of the chloride (molar ratio 1:25). The resulting powder is pressed into pellets placed above a platinum foil in an alumina boat. The pellets are then heated at

225°C for 20 h under argon flow with a heating rate of 180 °C/h. The exchange reaction which takes place corresponds to :



After cooling, the sample is rapidly washed with H₂O or D₂O (Euriso-top 99.9%) to dissolve the chloride excess and to eliminate the lithium exchanged. After filtration, the compound is dried at 110°C in an oven for LiHSrTa₂O₇ or at room temperature in a glove box for LiDSrTa₂O₇. A chemical analysis (flame photometry) of the lithium quantity in the filtrate confirms the ionic Li⁺/H⁺ exchange rate and consequently the chemical formulation LiHSrTa₂O₇ (LiDSrTa₂O₇). For more details, see reference 21.

2.2. Thermal powder diffraction data

In order to check the purity and the quality of the different phases, Li₂SrTa₂O₇, LiHSrTa₂O₇ and LiDSrTa₂O₇, powder X-ray diffraction data (PXRD) were collected in air at room temperature with a PANalytical X'pert Pro diffractometer equipped with the X'Celerator detector using CuK α radiation in 5-130°2 θ range with a 0.017° step scan increment and a counting time of 210 seconds per step. The thermal PXRD patterns, performed on LiHSrTa₂O₇, were collected with the same diffractometer completed with a high temperature attachment Anton Paar HTK12. They were recorded under N₂ flow between room temperature and 270°C in the range 8 - 130° 2 θ , with a step of 0.017° and a counting time of 130 seconds per step.

Concerning the neutron powder diffraction (NPD) patterns, they were registered on the deuterated specimen LiDSrTa₂O₇, at ILL on D2B high-resolution neutron diffractometer in the temperature range 25°C – 250°C with the following experimental conditions: $\lambda = 1.59431(1)$ Å, angular range (°2 θ) = 0.10-159.95; step scan increment (°2 θ) = 0.05, counting time = 5 h.

All the refinements were carried out by the Rietveld method²³ using Fullprof software²⁴ with a pseudo-Voigt function.

2.3. Thermal analysis

Differential Scanning Calorimetry (DSC) was performed on a TA instrument Q100 equipped with a refrigerated cooling system. The data, registered under heating and cooling, were obtained using a scan rate of 10°C/mn under N₂ flow between room temperature and 250°C. An isothermal step of 1 min was applied to ensure complete transformation and homogenization of the sample.

2.4. Second harmonic generation (SHG) test

The Second Harmonic Generation (SHG) test is commonly used as a proof of crystal non-centrosymmetry.²⁵ The short laser pulses (0.6 ns, 10 μ J at 1064 nm and 5 kHz repetition rate) of a microchip Q-switched Nd:YAG laser (Teem photonics) are focused by a microscope objective (X 6.3) onto the LiHSrTa₂O₇ powder sample introduced in a Lindemann capillary tube with 0.7 mm internal diameter. The back-scattered SHG light at 532 nm is collected and collimated by the same microscope objective used to focus the pump light. The residual pump light at 1064 nm back-scattered by the powder sample is completely rejected from the SHG light beam, firstly, by a dichroic mirror and secondly, by a narrow-bandpass optical filter centered at 532 nm. The SHG pulses are detected by a high-speed photo-receiver connected to a 3 GHz-bandpass digital oscilloscope for the measurement the SHG peak power.

The SHG efficiency is known to vary significantly near the temperature of a phase transition.²⁵ For the study in temperature, the Lindemann tube containing the LiHSrTa₂O₇ powder sample is introduced in a handmade micro-oven and the sample is heated between the ambient temperature to about 300 °C. The SHG peak power is measured in function of the sample temperature.

2.5. Raman experiments

Raman spectra were registered for LiHSrTa₂O₇ compound and obtained from compacted powder pellets placed in a lab-made cell²⁶ allowing temperature control from liquid N₂ to 600°C in a flowing dry synthetic air atmosphere. Low wavenumber spectra were acquired with a Jobin-Yvon T64000 spectrometer working in triple subtractive mode (entrance double stage monochromator in a subtractive mount plus spectrograph). High wavenumber spectra were obtained with a Renishaw InVia spectrometer equipped with dielectric filters. The photon counting system was a CCD cooled with liquid nitrogen (T64000) or with a Peltier module (InVia). In both cases, the excitation source was the green (514.53 nm) light of an argon laser.

3. Results

3.1. Thermal X-ray diffraction

One checked the good quality and the purity of the sample LiHSrTa₂O₇, PXRD patterns were recorded from room temperature (RT) to 270°C in order to obtain the thermal evolution of the cell parameters. This temperature range has been chosen from previous TGA results which clearly shows that LiHSrTa₂O₇ begins to decompose above 350°C leading at 700°C to a poorly crystallized mixture of SrTa₂O₆ and Li₂SrTa₂O₇ due to the total loss of proton as H₂O.²¹ According to the RT study²¹ and whatever the temperature between RT and 270°C, all the diffraction peaks of the PXRD patterns can be indexed in the Fmmm space group using

the following super cell : $a = \sqrt{2}a_p \approx 5.5 \text{ \AA}$, $b = \sqrt{2}a_p \approx 5.5 \text{ \AA}$ and $c \approx 18.8 \text{ \AA}$ (a_p being the cell parameter of the simple cubic perovskite ABO_3). At room temperature, the refined cell parameters are in good agreement with those obtained in reference 21. Under heating, the a parameter remains nearly constant while the b one regularly increases until it becomes equal to the a parameter around 210°C (Fig. 1a). This implies thus that a progressive structural transition occurs from the orthorhombic system to the tetragonal one. This is also clearly visible in figure 2 which represents the thermal evolution of the 200 and 020 lines: at RT, these two lines are clearly separated due to the orthorhombic distortion while they are superimposed from 225°C . Above this temperature, all the hkl lines of the PXRD pattern can be indexed in the $I4/mmm$ space group, with a smaller cell $a = b \approx a_p \approx 3.9 \text{ \AA}$ and $c \approx 18.8 \text{ \AA}$. In parallel, the c parameter varies accidentally (Fig. 1-b), increasing until $T \leq 125^\circ\text{C}$ before decreasing for $125^\circ\text{C} \leq T \leq 230^\circ\text{C}$ and increasing again above 230°C . Nevertheless, in spite of this behavior, the cell volume globally increases with however an accident for $125^\circ\text{C} < T < 175^\circ\text{C}$ (Fig. 1-c).

3.2. DSC experiment

The DSC study has been performed from room temperature to 250°C , this temperature range avoiding the decomposition of $\text{LiHSrTa}_2\text{O}_7$. The heating and cooling curves (Fig. 3) show two very close endothermic peaks around 197 and 215°C , both of them being associated with reversible phenomena.

3.3. Thermal SHG

As the structure of $\text{LiHSrTa}_2\text{O}_7$ is non centrosymmetric at room temperature,²¹ we decided to complete the thermal study by following the intensity of the SHG signal versus temperature (Fig. 4) under heating and cooling. The obtained curves confirm the acentric character of the structure at room temperature and show that under heating, the intensity of the SHG signal decreases. At 235°C , the SHG signal completely vanishes, indicating thus that $\text{LiHSrTa}_2\text{O}_7$ undergoes a structural transition around this temperature. This transition is reversible since a positive SHG response is rapidly restored when the sample is cooled (Fig. 4).

3.4. Raman experiments

The figure 5 shows the Raman spectra obtained at various temperatures between 107 K (-166°C) and 573 K (300°C). At low temperatures, the Raman spectra are characterized by a large number of bands, in agreement with the complex structure of $\text{LiHSrTa}_2\text{O}_7$ at room temperature²¹ (SG : $\text{Ama}2$). Above 3000 cm^{-1} , a narrow and rather intense band at 3495 cm^{-1} is characteristic of an O-H bond with a short bond length. A shoulder near 3420 cm^{-1} is also observed, characteristic of a longer O-H bond. Two bands at 1375 and 1585 cm^{-1} can be

attributed to the vibration of the corresponding O--H hydrogen bonds. These results are in agreement with the RT neutron diffraction study of Galven et al.²¹ who showed the existence of two sites for the hydrogen atoms, each approximately half-filled, with an O-H distance of 0.86 and 1.04 Å, respectively. However, the O-H distances deduced from spectroscopic data, reference 27 and references herein, correspond better to 0.97 and 1.00 Å, respectively. A complex band near 900 cm⁻¹ is characteristic of a short Ta-O bond, shorter than in Li₂SrTa₂O₇.²⁰ This band corresponds to the stretching of the short Ta-O₃ bond of the Ama2 structure.

Under heating, we observe a progressive evolution of the Raman spectra between 170 and 200°C. This evolution is characterized by the disappearance of many bands as expected from symmetry consideration, confirming thus the existence of a structural transition around these temperatures. The progressive character of the transition is confirmed by the observation of a mixture of regions for which the transition already occurred and regions still in the low temperature phase. Due to the transition, the O-H stretching region (3000-3500 cm⁻¹) and the high wavenumber part of the Ta-O stretching region (800-900 cm⁻¹) show interesting behaviors. Indeed, the strong Ta-O stretching band corresponding to a short Ta-O bond at 890-900 cm⁻¹ decreases markedly being progressively replaced by the 800-850 cm⁻¹ bands. The short Ta₂-O₃ bond thus disappears at the transition, replaced by a longer bond which length is near that of the shortest Ta₂-O bonds. Also, the narrow and intense O-H band located at 3495 cm⁻¹ in the low temperature spectra disappears at the transition. The two kinds of O-H bonds observed in the low temperature phase are replaced by a single one at high temperature. The resulting stretching frequency corresponds to the longest O-H bond of the low temperature phase. This can be interpreted as a more ionic character of the O-H bond. The role of hydrogen becomes thus closer to that of lithium. The softening of the strong O-H bond could thus be the driving force for the phase transition.

At 250°C, the Raman spectrum of LiHSrTa₂O₇ (Fig. 6) is very close to that of the high temperature Li₂SrTa₂O₇ form which crystallizes in the I4/mmm space group. The major differences are an enlargement of all bands, the shift of the short Ta-O bond stretching frequency (near 800 cm⁻¹) towards slightly high wavenumbers, and the corresponding shift of the Li(H)-O stretching frequencies (320-370 cm⁻¹ in Li₂SrTa₂O₇) towards lower wavenumbers. The enlargement corresponds to the disorder in the Li(H) sites, and the largest changes in frequency also imply the oxygen atoms in contact with these cations.

Finally and in addition to the DSC study, the reversibility of the structural transition is confirmed since the Raman spectrum at 25°C is the same before and after the high temperature measurements (Fig. 5-b).

3.5. Thermal neutron diffraction

In reference 21, we have shown from NPD data analysis that the acentric character of $\text{LiHSrTa}_2\text{O}_7$ ($\text{LiDSrTa}_2\text{O}_7$) at room temperature is mainly due to the special Li^+/H^+ (Li^+/D^+) distribution. Indeed, Li^+ and D^+ cations are unequally distributed on different sites in the interlayer spacing: two 4a sites for Li^+ cations (partially occupied at 69 and 31%) and two 4b sites for D^+ ions (partially occupied at 60 and 40%). Taking into account the transitions highlighted from the DSC, SHG and Raman experiments, we suspect that under heating, a reordering of Li^+ and D^+ ions takes place inside the preserved layered perovskite framework. We decided then to follow the structural evolution of $\text{LiDSrTa}_2\text{O}_7$ versus temperature using neutron diffraction since it is more sensitive for the precise location of light atoms like lithium, deuterium and oxygen in compounds containing heavy chemical elements as tantalum and strontium.

Taking into account the time required to record the data at each temperature (5 hours) and the temperature corresponding to the decomposition beginning (about 350°C), we chose to collect NPD data at three temperatures 25, 160 and 250°C. A part view of the resulting patterns are presenting in figure 7. It reveals first that the structures of the low and the high temperature forms are strongly correlated since the corresponding NPD patterns are quite similar. A careful examination reveals in addition that some (hkl) lines disappear under heating indicating thus that the compound undergoes a structural transition. In order to follow the structural evolution with the temperature under the best conditions, we decided for the room temperature refinement to start with the structural Ama2 model of reference 21 and with the same D-O soft constraints (1.00 with 0.05 Å standard error). The occupation factors of the two Li sites and the two D sites are refined independently with only a global constraint to the nominal value (4 lithium atoms and 4 deuterium atoms per unit-cell). In these conditions, this new set of results at 25°C is in very good agreement with the reference 21, especially the Li^+/D^+ distribution (Tables 1 and 2). Indeed, the four lithium cations and the four deuterium cations are both unequally distributed over their sites: 67% on the Li1 site and 33% in the Li2 site (compared to 69% and 31% respectively in reference 21); 58% on the D1 site and 42% on the D2 site (compared to 60% and 40% respectively in reference 21).

At 160°C, as the SHG signal is still visible, the refinement was performed starting from the refined 25°C model in the Ama2 space group. It converged quickly towards good reliability

factors (table 1) and the agreement between the observed and the calculated patterns is very satisfactory (Fig. 8).

At 250°C, the refinement has been undertaken in the I4/mmm space group using the following cell $a = b \approx a_p \approx 3.93 \text{ \AA}$ and $c \approx 18.77 \text{ \AA}$. This space group has been chosen taking into account the thermal X-ray diffraction study which showed that LiHSrTa₂O₇ undergoes a structural transition from an orthorhombic to a tetragonal symmetry. In addition, the Raman spectra of the high temperature form is very close to that of the high temperature Li₂SrTa₂O₇ form which crystallizes in the I4/mmm space group. All the *hkl* lines being well indexed in this configuration, we used the atomic model of the perovskite blocks [SrTa₂O₇]²⁻ taken from reference 20. Fourier difference calculations²⁸ are used to complete the structure when the refined [SrTa₂O₇]²⁻ atomic positions are judged to be stabilized. Two crystallographic sites are then found: one site 4d for Li⁺ (0, 0.50, 0.25) and one site 16m for D⁺ (0.65, 0.65, 0.24). Taking into account the number of *hkl* compared to the number of refined parameters, we decided to applied anisotropic temperature factors for all atoms but to fix the Li⁺ and D⁺ occupation factors to their nominal values (2 lithium and 2 deuterium atoms per unit-cell) since there is only one site for each. In these conditions, the reliability factors decreases significantly towards very good values (table 1). The figure 9 shows the observed, calculated and difference of the corresponding NPD pattern.

All these NPD results are gathered in the table 1 for the structure refinement results, table 2 and table 3 for the atomic coordinates, Biso and bond valence sums respectively in the space groups Ama2 (RT and 160°C) and I4/mmm (250°C), while table 4 includes all the main interatomic distances.

4. Discussion

All the studies previously described show unambiguously that LiHSrTa₂O₇ undergoes a reversible structural transition near 200°C: the SHG signal which progressively vanishes under heating completely disappears above 235°C; the thermal evolution of the *a* and *b* cell parameters indicates that the structure of the compound changes from an orthorhombic to a tetragonal symmetry around 210°C. This transition toward a tetragonal symmetry is also supported by the similarity of the Raman spectra of LiHSrTa₂O₇ at 250°C and of Li₂SrTa₂O₇ at 410°C, this former crystallizing in the I4/mmm space group. In addition, the NPD pattern at 250°C is perfectly refined in I4/mmm.

In these conditions, why the DSC curve shows two peaks, one around 197°C and the second one near 215°C ? The existence of these two reversible peaks implies that LiHSrTa₂O₇ undergoes two reversible transformations under heating. Unfortunately, as the peaks are very

close to one another, it is extremely difficult to isolate the intermediate $\text{LiHSrTa}_2\text{O}_7$ form and to explain the first transition. Then, the transition toward the $I4/mmm$ variety can be unambiguously associated to the second peak. Concerning the first one, we can nevertheless make a hypothesis. Indeed, during our structural study on the parent $\text{Li}_2\text{SrTa}_2\text{O}_7$,²⁰ we have shown that at 230°C this compound undergoes a structural transition from Cmcm to $I4/mmm$. As Ama2 is a subgroup of Cmcm , it is possible that $\text{LiHSrTa}_2\text{O}_7$ transforms from Ama2 to Cmcm (first transition at 197°C) and then from Cmcm to $I4/mmm$ (second transition at 215°C). From a structural point of view, the first transition (Ama2 to Cmcm) should correspond to an equal distribution of the Li^+ and H^+ (D^+) cations on their two respective sites while remaining in the orthorhombic system.

Despite we do not have structural information on the intermediate form, we can nevertheless follow the structural evolution of $\text{LiDSrTa}_2\text{O}_7$ from RT (Ama2) to 250°C ($I4/mmm$) from NPD data. Figure 10 represents the $\text{LiDSrTa}_2\text{O}_7$ structures at RT, 160°C and 250°C . Whatever the temperature (RT, 160°C and 250°C), the structures are closely related to RP phases with $n = 2$ meaning that two adjacent perovskite blocks are linked together by lithium and deuterium atoms. These atoms are then located in the interlayer spacing while the larger strontium atoms fully occupy the twelve coordinated perovskite cages. All the mean distances cation-anion observed (table 4) are in good agreement with the sum of the ionic radii from Shannon's table,²⁹ leading consequently to bond valence sums^{30,31} close to the expected values (tables 2 and 3). Concerning the apical oxygen (O2 and O3) bond valence calculations, the situation is more complex due to the presence of vacancies on the Li and D sites and to short distances Li1-D2 and Li2-D1 (close to 1.5 \AA). This implies firstly that the distances O2-Li(D) and O3-Li(D) are necessarily locally slightly different from the values obtained from the NPD and secondly that different cationic environments are possible. For example, at 160°C , four possible environments must be considered leading to bond valence sums between 1.4 and 1.9 for O2 and 2.1 and 2.5 for O3 .

Usually in the layered perovskite phases, the central atom of the octahedra BO_6 occupies an off-centered position. In the case of $\text{LiDSrTa}_2\text{O}_7$, the two different tantalum sites evidenced at RT and 160°C are not equivalent from this point of view. Indeed, if Ta1 is nearly at the centre of the corresponding Ta1O_6 octahedra, Ta2 is very displaced from the centre of the Ta2O_6 octahedra by about 0.32 and 0.33 \AA respectively. At 250°C , there is only one tantalum site with a significantly decreased displacement (0.17 \AA). As expected in the case of an off-centered position, the shortest Ta2-O distance corresponds to the linkage with the terminal oxygen (O3).

The main consequence of the temperature relies on the Li^+ and D^+ populations in the interlayer spacing. In the RT form, Li^+ and D^+ cations are unequally distributed on different sites in the interlayer spacing: two 4a sites for Li^+ cations (partially occupied at 67 and 33%) and two 4b sites for D^+ ions (partially occupied at 58 and 42%) (table 2). At 160°C, the unequal lithium distribution is preserved, while a balance of the deuterium population is nearly reached since the occupation of the two 4b sites is close to 50% (table 2). At 250°C, the balance of population is reached for both cation types (Table 3): the two 4a sites of lithium become the 4d site in the $I4/mmm$ space group (occupation factor equal to 0.5) and the two 4b sites of deuterium become the 16m site in the $I4/mmm$ space group (occupation factor equal to 0.125). This implies that the displacement of lithium and deuterium is driven by the heating and leads towards a progressive population balance of these two cations with a regular distribution in the interlayer spacing. In our previous RT study,²¹ we showed that the acentric character is mainly driven by the unequal Li^+/D^+ distribution. In this new study, the progressive disappearance of the SHG signal with temperature can be directly associated with the displacement of Li^+ and D^+ cations inside a nearly preserved $[\text{SrTa}_2\text{O}_7]^{2-}$ framework. Moreover, such reorganization is reversible according to the results obtained by the experimental techniques used in this paper. The first transition from $Ama2$ to $Cmcm$, proposed above, is then all the more likely that thermal NPD experiments showed that the Li^+/D^+ distribution is directly affected by the temperature factor.

For RT and 160°C, we can see figure 10 that the TaO_6 octahedra are slightly tilted due to small displacements of the oxygen atoms. As a result, the octahedra tilting brings closer the oxygen O4 (of the equatorial plane) of Li2 so that it could be taken into account in the lithium environment structural description: respectively at 2.22 and 2.36 Å leading to a five coordinence. At 250°C, the octahedra are completely aligned. This moves the O4 oxygen away from the lithium environment, the distance Li2-O4 being then close to 2.77 Å. The coordinence is then tetrahedral. Consequently to this straightening, the thickness of the blocks slightly increases from 8.003 (RT) to 8.028 Å (250°C) with however a mean Ta-O distance similar for the three studied temperatures (table 4). In parallel, a shrinking of the interlayer spacing (the interlayer spacing being calculated from the difference of the z-coordinates of the two apical oxygen atoms in adjacent perovskite slabs) is observed, from 1.386 (RT), 1.384 Å (160°C) and to 1.358 Å at 250°C. These variations are mainly due to the change of the Li^+ and D^+ distribution in the interlayer spacing as the shift of two successive blocks remains the same whatever the temperature (I mode). The competition of these two opposite variations in addition to the thermal expansion leads to the non regular evolution of the c parameter.

5. Conclusion

A thermal structural characterization of the acentric layered perovskite $\text{LiHSrTa}_2\text{O}_7$ ($\text{LiDSrTa}_2\text{O}_7$) has been performed with several complementary techniques: powder X-ray and neutron diffraction, DSC, SHG and Raman experiments.

The PXRD patterns evolution shows that the orthorhombic distortion, clearly visible at RT, progressively vanishes when the temperature increases, leading to a tetragonal symmetry above 210°C. DSC, SHG tests and Raman experiments prove unambiguously the reversibility of the phase transition, while Raman results allow to propose the $I4/mmm$ space group to describe the structure of the high temperature form.

These results are confirmed by NPD data refinement at RT, 160°C and 250°C since at RT and 160°C, the NPD pattern can be refined in the $Ama2$ space group ($a = \sqrt{2}a_p \approx 5.5 \text{ \AA}$, $b = \sqrt{2}a_p \approx 5.5 \text{ \AA}$ and $c \approx 18.8 \text{ \AA}$), while at 250°C, the $I4/mmm$ space group with a smaller cell ($a = b \approx a_p \approx 3.9 \text{ \AA}$ and $c \approx 18.8 \text{ \AA}$) is enough to refine successfully the pattern observed. Whatever the temperature, two successive perovskite blocks remain stacked with an I mode fashion. Below the structural transition temperature, the octahedra are tilted inside these blocks leading to a [4+1] coordination for the lithium cations. In the high temperature form, the tilting disappears leading to octahedra perfectly straightened and to a tetrahedral environment for lithium ions built by four apical oxygen ions of two successive slabs. In addition to these changes, the heating allows a displacement of Li^+ and D^+ cations in the interlayer spacing. Above the structural transition, these two cations are regularly distributed over their available sites, this leading consequently to the disappearance of the acentric character of the structure.

To close this work, it could be interesting to study the ionic conduction as we have shown that Li^+ and D^+ cations are moving under heating. However, $\text{LiHSrTa}_2\text{O}_7$ is stable only under 350°C, this behavior preventing then to perform measurements on sintered pellets with high compacity.

Acknowledgements:

The authors thank J. Y. Botquelen (Institut des Molécules et Matériaux du Mans) and V. Pagot and A. Riot (ENSIM students) for SHG measurements.

References

- 1 S. N. Ruddlesden and P. Popper, *Acta Crystallogr.*, 1957, **10**, 538
- 2 S. N. Ruddlesden and P. Popper, *Acta Crystallogr.*, 1958, **11**, 54
- 3 K. Toda, J. Watanabe and M. Sato, *Mater. Res. Bull.*, 1996, **31 (11)**, 1427
- 4 M. Sato, T. Jin and H. Ueda, *Chem. Lett.* 1994, 161
- 5 M. Richard, L. Brohan and M. Tournoux, *J. Solid State Chem.*, 1994, **112**, 345
- 6 P. J. Ollivier and T. E. Mallouk, *Chem. Mater.*, 1998, **10**, 2585
- 7 N. S. P. Bhuvanesh, M. P. Crosnier-Lopez, H. Duroy and J. L. Fourquet, *J. Mater. Chem.*, 1999, **9**, 3093
- 8 N. Floros, C. Michel, M. Hervieu and B. Raveau, *J. Mater. Chem.*, 1999, **9**, 3101
- 9 T. A. Kodenkandath, J. B. Wiley, *Mater. Res. Bull.*, 2000, **35**, 1737
- 10 M. P. Crosnier-Lopez, F. Le Berre and J. L. Fourquet, *Z. Anorg. Allg. Chem.*, 2002, **628**, 2049
- 11 N. S. P. Bhuvanesh, M. P. Crosnier-Lopez, O. Bohnke, J. Emery and J. L. Fourquet, *Chem. Mater.*, 1999, **11**, 634
- 12 F. Le Berre, M. P. Crosnier-Lopez, Y. Laligant, E. Suard, O. Bohnke, J. Emery and J. L. Fourquet, *J. Mater. Chem.*, 2004, **14**, 3558
- 13 S. Ikeda, M. Hara, J. N. Kondo and K. Domen, *Chem. Mater.*, 1998, **10**, 72-77
- 14 W. Yao and J. Ye, *Chem. Phys. Lett.*, 2007, **435**, 96
- 15 F. E. Osterloh, *Chem. Mater.* 2008, **20**, 35
- 16 Y. Wei, J. Li, Y. Huang, M. Huang, J. Lin and J. Wu, *Solar Energy Materials and Solar cells*, 2009, **93**, 1176
- 17 Y. Huang, Y. Wei, S. Cheng, L. Fan, Y. Li, J. Lin and J. Wu, *Solar Energy Materials and Solar cells*, 2010, **94**, 761
- 18 J. A. Schottenfeld, Y. Kobayashi, J. Wang, D. D. Macdonald and T.E. Mallouk, *Chem. Mater.*, 2008, **20**, 213
- 19 R. E. Schaak and T.E. Mallouk, *Chem. Mater.*, 2000, **12**, 3427
- 20 T. Pagnier, N. Rosman, . Galven, E. Suard, J. L. Fourquet, F. Le Berre and M. P. Crosnier-Lopez, *J. Solid State Chem.*, 2009, **182**, 317
- 21 C. Galven, J. L. Fourquet, E. Suard, M. P. Crosnier-Lopez and F. le Berre, *Dalton Trans.*, 2010, **39**, 3212
- 22 N. S. P. Bhuvanesh, M. P. Crosnier-Lopez, H. Duroy and J. L. Fourquet, *J. Mater. Chem.*, 2000, **10**, 1685

- 23 H. M. Rietveld, *J. Appl. Crystallogr.*, 1969, **2**, 65
- 24 J. Rodriguez-Carvajal, Program FULLPROF.2K, Version 5.30, 2012, Institut Laüe-Langevin, Grenoble.
- 25 J. P. Dougherty, S. K. Kurtz, *J. Appl. Cryst.*, 1976, **9**, 145-158.
- 26 O. Sze Nga Sum , E. Djurado, T. Pagnier, N. Rosman , C. Roux and E. Siebert, *Solid State Ionics*, 2005, **76**, 2599
- 27 A. Novak in *Hydrogen bonding in solids. Correlation of spectroscopic and crystallographic data, Vol. 18* Springer, Berlin, **1974**, 177
- 28 J. Gonzales-Platas and J. Rodriguez-Carvajal, Program GFOURIER, version 4.06, 2007, Institut Laüe-Langevin, Grenoble
- 29 R. D. Shannon, *Acta Crystallogr. Sect. A: Cryst. Phys., Diffr., Theor. Gen. Cryst.*, 1973, **32**, 751
- 30 N.E. Brese and M. O'Keeffe, *Acta Crystallogr. Sect. B: Struct. Sci.*, 1991, **47**, 192
- 31 I.D. Brown, Private Communication, LLB, version: February 2010, bound to Fullprof

Figure captions

Fig. 1 : Cell parameters and volume evolution versus temperature ($25^{\circ}\text{C} \leq T \leq 270^{\circ}\text{C}$) for $\text{LiHSrTa}_2\text{O}_7$ from PXRD data refinement. For the tetragonal cell ($T \geq 225^{\circ}\text{C}$), the a and b parameters are multiplied by $\sqrt{2}$ for the volume calculation (T_s : structural transition temperature from orthorhombic to tetragonal).

Fig. 2 : Selected part of the PXRD patterns showing the progressive vanishing of the orthorhombic distortion versus temperature on the 200 and 020 lines.

Fig. 3 : DSC curve for $\text{LiHSrTa}_2\text{O}_7$ under heating and cooling.

Fig. 4 : Evolution of the SHG signal intensity versus temperature for $\text{LiHSrTa}_2\text{O}_7$.

Fig. 5 : Raman spectra obtained as a function of temperature with the Jobin-Yvon T6400 spectrometer (a) or the Renishaw InVia spectrometer (b). The top spectrum of fig. 5b is obtained after going back to 25°C , showing the reversibility of the phase transition.

Fig. 6 : Raman spectra of $\text{Li}_2\text{SrTa}_2\text{O}_7$ at 410°C and $\text{LiHSrTa}_2\text{O}_7$ at 350°C . The star indicates a spurious band (light from the computer screen).

Fig. 7 : Selected part of the NPD patterns showing the disappearance of some lines (*) under heating for $\text{LiDSrTa}_2\text{O}_7$.

Fig. 8 : Observed, calculated and difference NPD patterns of $\text{LiDSrTa}_2\text{O}_7$ at 160°C in the Ama2 space group. Vertical bars are related to the calculated Bragg reflection positions.

Fig. 9 : Observed, calculated and difference NPD patterns of $\text{LiDSrTa}_2\text{O}_7$ at 250°C in the I4/mmm space group. Vertical bars are related to the calculated Bragg reflection positions

Fig. 10 : Projections of the $\text{LiDSrTa}_2\text{O}_7$ structure on the (1 -1 0) plane (RT and 160°C) and on the (1 0 0) plane (250°C).

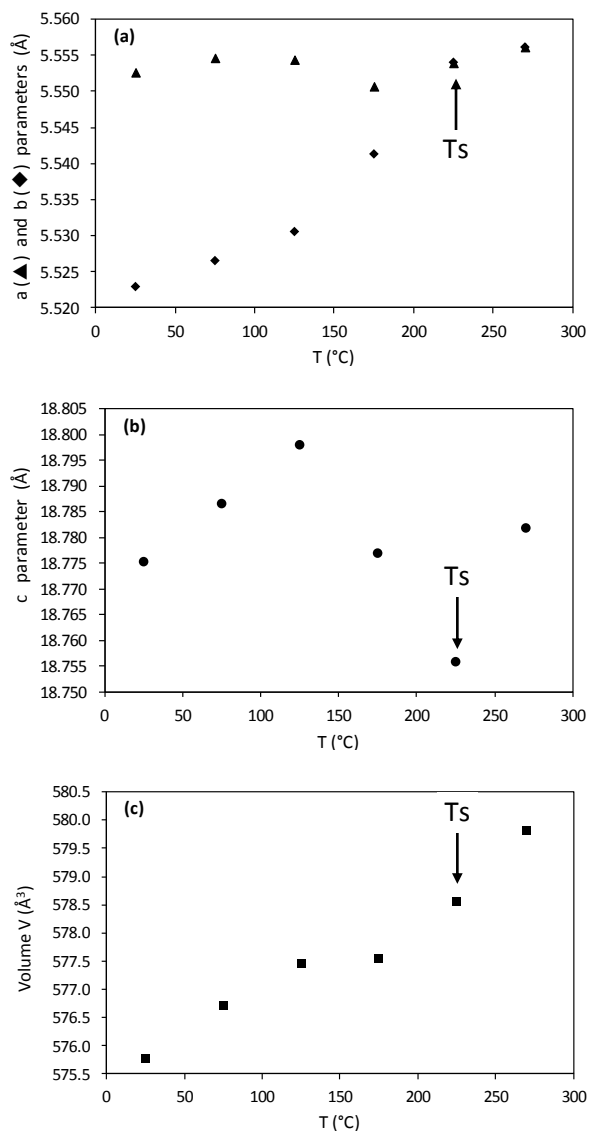


Figure 1 : Cell parameters and volume evolution versus temperature ($25^\circ\text{C} \leq T \leq 270^\circ\text{C}$) for $\text{LiHSrTa}_2\text{O}_7$ from PXRD data refinement. For the tetragonal cell ($T \geq 225^\circ\text{C}$), the a and b parameters are multiplied by $\sqrt{2}$ for the volume calculation. (T_s : structural transition temperature from orthorhombic to tetragonal)

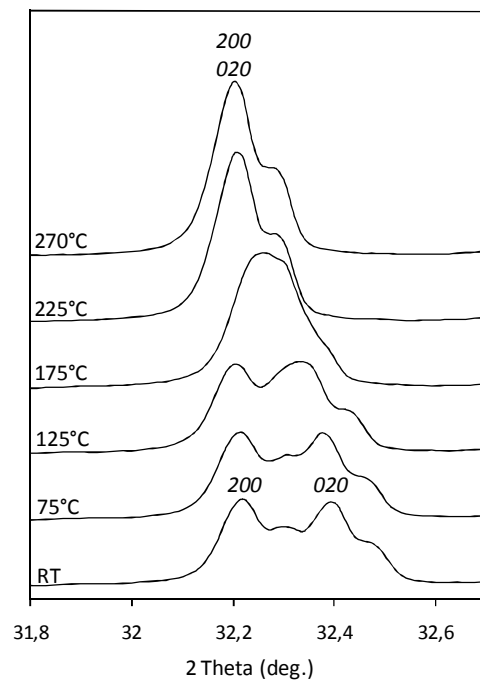


Figure 2 : Selected part of the PXRD patterns showing the progressive vanishing of the orthorhombic distortion versus temperature on the *200* and *020* lines.

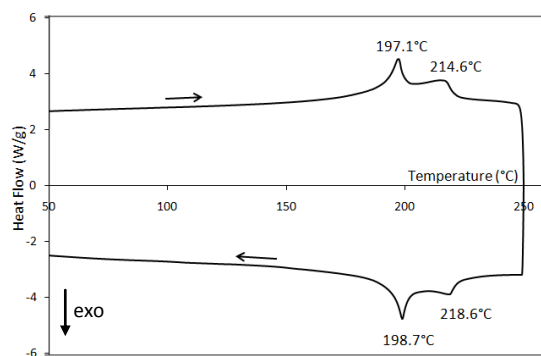


Figure 3 : DSC curve for LiHSrTa₂O₇ under heating and cooling

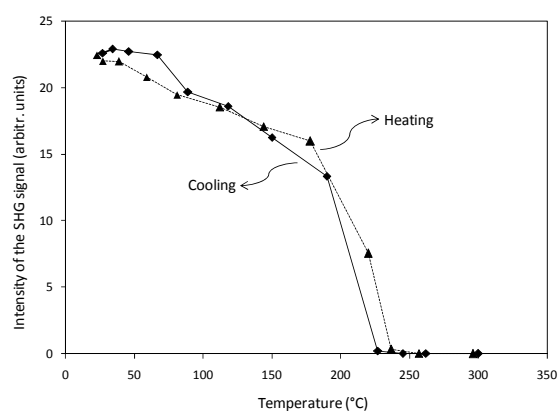


Figure 4: Evolution of the SHG signal intensity versus temperature for LiHSrTa₂O₇

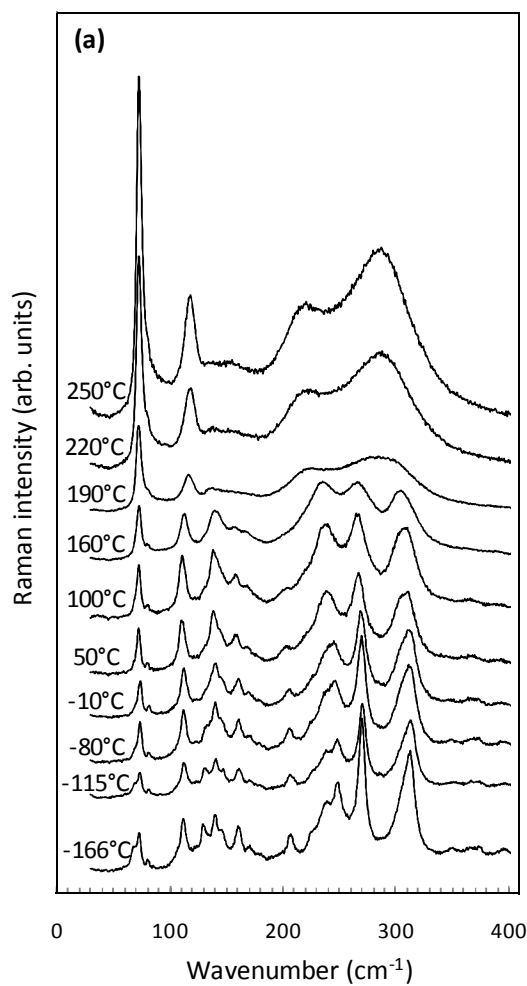
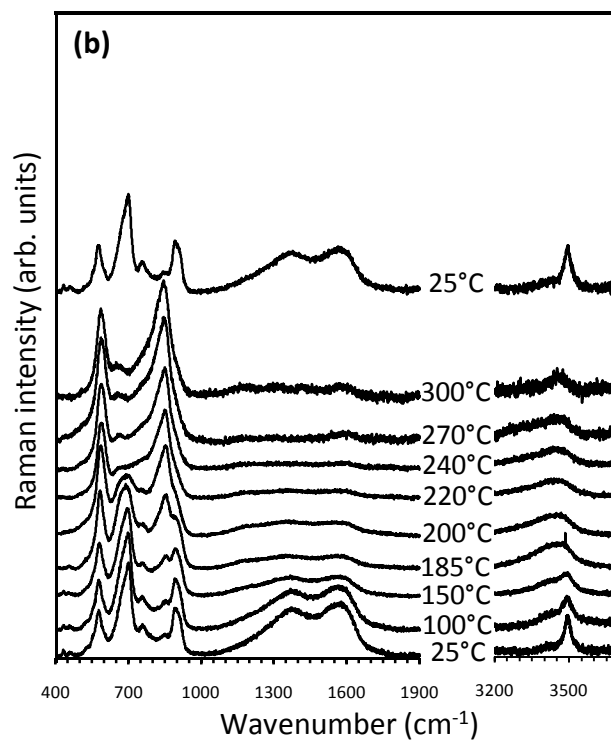


Figure 5: Raman spectra obtained as a function of temperature with the Jobin-Yvon T6400 spectrometer (a) or the Renishaw InVia spectrometer (b). The top spectrum of fig. 5 b is obtained after going back to 25°C, showing the reversibility of the phase transition.



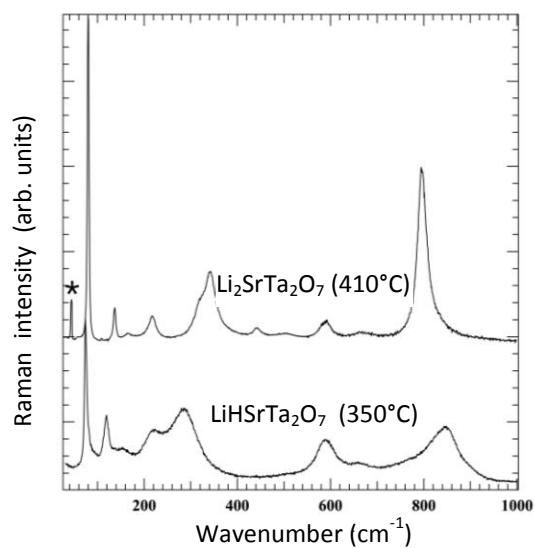


Figure 6: Raman spectra of $\text{Li}_2\text{SrTa}_2\text{O}_7$ at 410°C and $\text{LiHSrTa}_2\text{O}_7$ at 350°C.

The star indicates a spurious band (light from the computer screen)

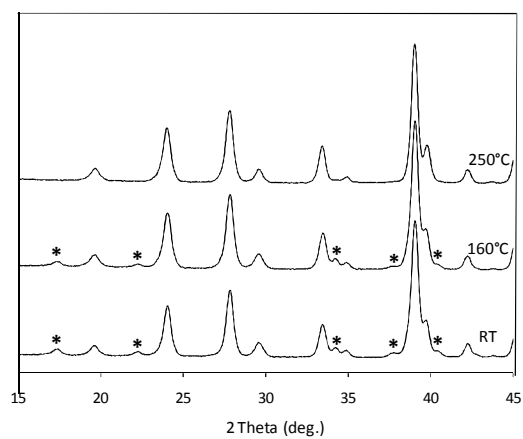


Figure 7 : Selected part of the NPD patterns showing the progressive disappearance of some lines (*) under heating for $\text{LiDSrTa}_2\text{O}_7$.

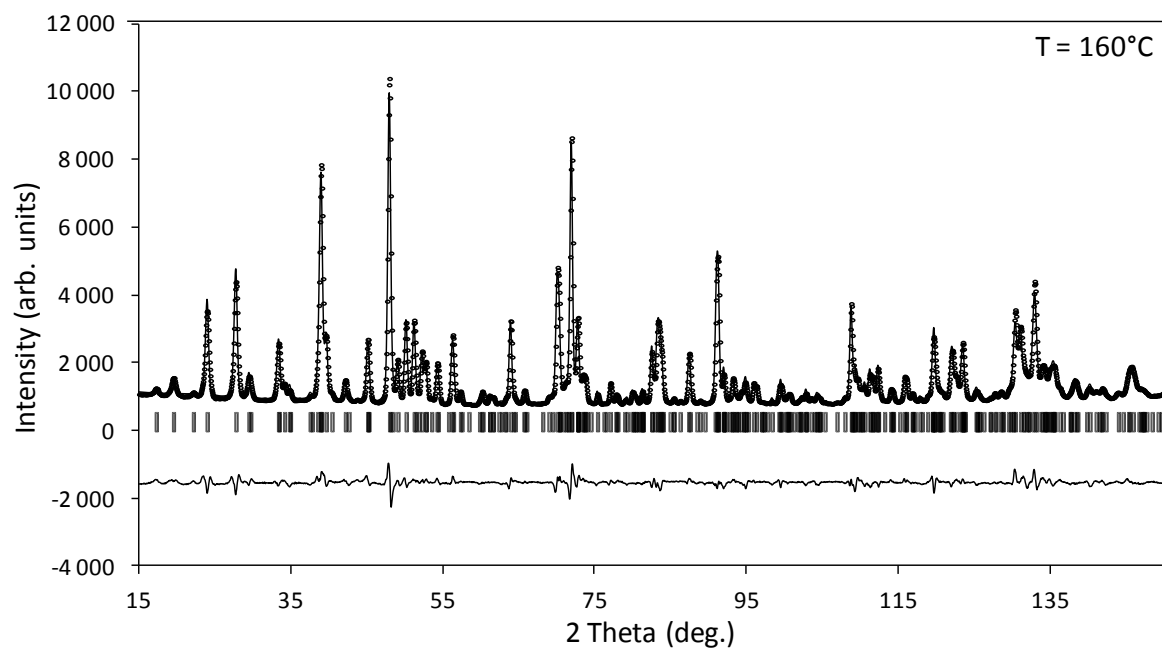


Figure 8 : Observed, calculated and difference NPD patterns of $\text{LiSrTa}_2\text{O}_7$ at 160°C in the Ama2 space group. Vertical bars are related to the calculated Bragg reflection positions

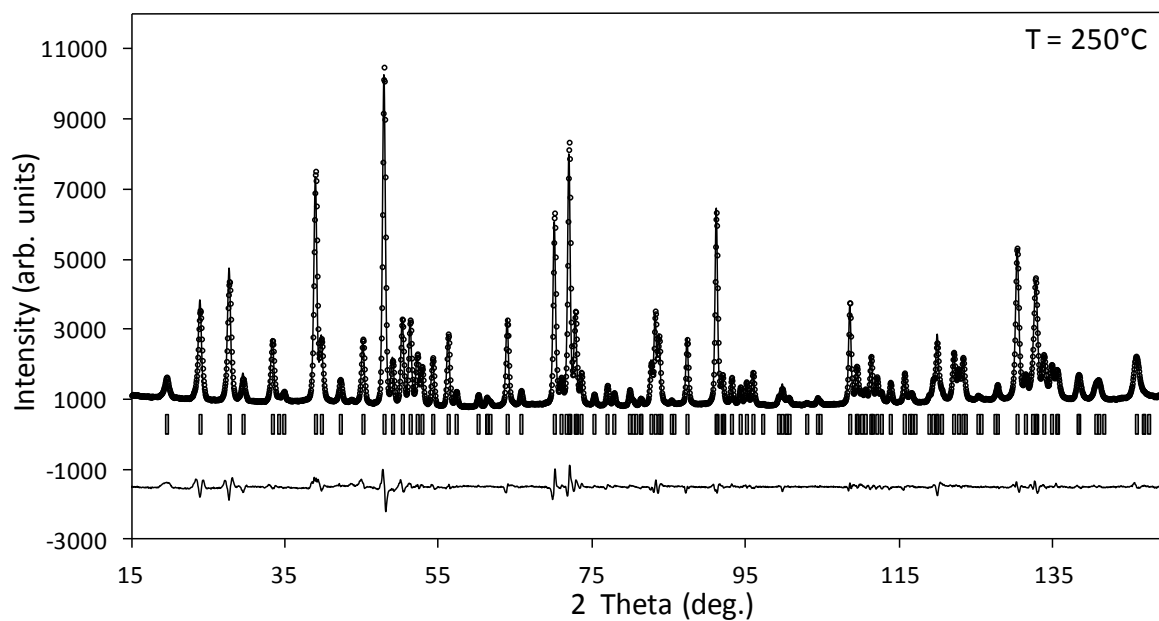


Figure 9 : Observed, calculated and difference NPD patterns of $\text{LiSrTa}_2\text{O}_7$ at 250°C in the $I4/mmm$ space group. Vertical bars are related to the calculated Bragg reflection positions

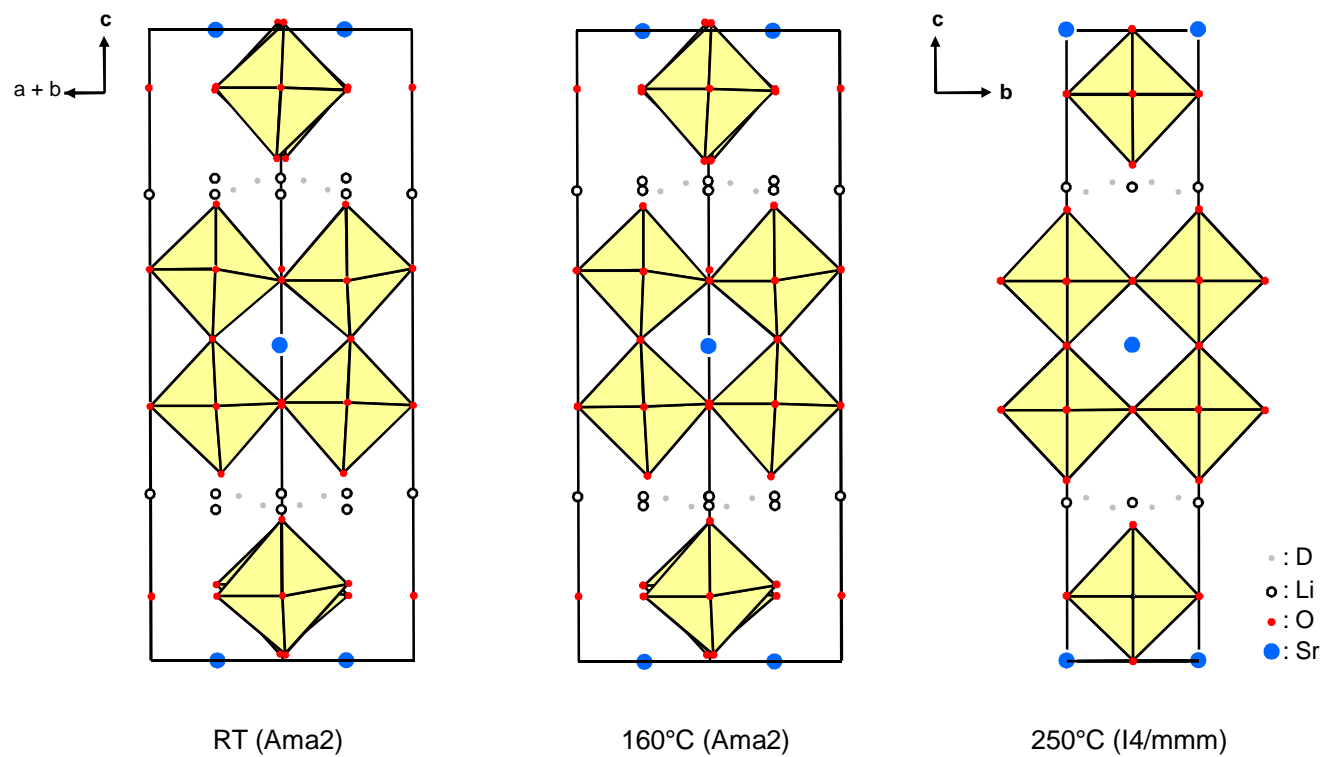


Figure 10 : Projection of the $\text{LiDSrTa}_2\text{O}_7$ structure on the (1 -1 0) plane (RT and 160°C) and on the (1 0 0) plane (250°C)

Table 1: Structure refinement results of $\text{LiDSrTa}_2\text{O}_7$ from neutron diffraction data

Temperature	RT	160°C	250°C
Space group	Ama2 (no. 40)	Ama2 (no. 40)	I4/mmm (no. 139)
Number of refined parameters	65	65	51
Peak shape, η	Pseudo-Voigt, 0.44(3)	0.34(3)	0.35(2)
Cell parameters/ Å	a = 5.5530(1)	5.5560(1)	3.9292(1)
	b = 5.5258(1)	5.5373(1)	
	c = 18.7767(4)	18.8027(3)	18.7716(3)
Cell volume/Z	576.2(2) Å ³ / Z = 4	578.5(2) Å ³ / Z = 4	289.8(2) Å ³ / Z = 2
Halfwidth parameters	u = 0.162(4)	0.134(4)	0.122(2)
	v = -0.332(9)	-0.292(9)	-0.279(6)
	w = 0.298(5)	0.299(5)	0.288(3)
	x = 0.0006(4)	0.0016(4)	0.0013(3)
Asymmetry parameters	P ₁ = 0.023(7)	0.034(7)	0.042(5)
	P ₂ = 0.016(3)	0.018(3)	0.017(2)
R _{Bragg}	4.19	4.10	2.65
R _p	9.39	9.50	8.37
R _{wp}	10.30	9.94	8.82
R _{exp}	1.71	1.85	2.00
χ^2	35.8	28.8	19.5

Table 2: Atomic coordinates, B_{iso} and bond valence sums (Σ) for $\text{LiDSrTa}_2\text{O}_7$ from neutron diffraction data (S.G.: Ama2) at room temperature (in italics) and 160°C

	Site	s.o.f.	x	y	z	B (\AA^2)	Σ	(Σ_{exp})
Ta1	<i>4b</i>	<i>1</i>	<i>0.25</i>	<i>0.743(1)</i>	<i>0.1130</i>	<i>0.74(7)</i>	<i>5.2</i>	(5)
		1	0.25	0.745(1)	0.1130	0.78(7)	5.3	
Ta2	<i>4b</i>	<i>1</i>	<i>0.25</i>	<i>0.753(1)</i>	<i>0.8875(2)</i>	<i>0.54(7)</i>	<i>5.4</i>	(5)
		1	0.25	0.751(1)	0.8869(2)	1.11(8)	5.2	
Sr	<i>4b</i>	<i>1</i>	<i>0.25</i>	<i>0.260(1)</i>	<i>-0.0015(3)</i>	<i>0.85(5)</i>	<i>2.3</i>	(2)
		1	0.25	0.255(1)	-0.0018(3)	1.40(5)	2.2	
O1	<i>4b</i>	<i>1</i>	<i>0.25</i>	<i>0.727(1)</i>	<i>0.0096(4)</i>	<i>1.19(8)</i>	<i>2.0</i>	(2)
		1	0.25	0.729(1)	0.0104(4)	1.65(8)	2.0	
O2	<i>4b</i>	<i>1</i>	<i>0.25</i>	<i>0.755(2)</i>	<i>0.2220(4)</i>	<i>0.57(8)</i>	<i>(a)</i>	(2)
		1	0.25	0.752(2)	0.2203(4)	1.5(1)	(a)	
O3	<i>4b</i>	<i>1</i>	<i>0.25</i>	<i>0.785(1)</i>	<i>0.7959(4)</i>	<i>1.5(1)</i>	<i>(a)</i>	(2)
		1	0.25	0.780(1)	0.7940(4)	2.2(1)	(a)	
O4	<i>4a</i>	<i>1</i>	<i>0.00</i>	<i>0.00</i>	<i>0.6200(4)</i>	<i>0.7(1)</i>	<i>2.1</i>	(2)
		1	0.00	0.00	0.6197(4)	1.1(1)	2.1	
O5	<i>4a</i>	<i>1</i>	<i>0.00</i>	<i>0.00</i>	<i>0.4033(4)</i>	<i>0.9(1)</i>	<i>2.2</i>	(2)
		1	0.00	0.00	0.4036(4)	0.9(1)	2.1	
O6	<i>4a</i>	<i>1</i>	<i>0.00</i>	<i>0.00</i>	<i>0.1017(4)</i>	<i>0.9(1)</i>	<i>2.0</i>	(2)
		1	0.00	0.00	0.1027(4)	1.7(2)	2.0	
O7	<i>4a</i>	<i>1</i>	<i>0.00</i>	<i>0.00</i>	<i>0.9077(4)</i>	<i>1.1(1)</i>	<i>2.2</i>	(2)
		1	0.00	0.00	0.9073(4)	1.7(2)	2.2	
Li1	<i>4a</i>	<i>0.67(6)</i>	<i>0.00</i>	<i>0.00</i>	<i>0.263(1)</i>	<i>0.5(2)</i>	<i>0.7</i>	(1)
		0.66(6)	0.00	0.00	0.260(2)	2.4(3)	0.7	
Li2	<i>4a</i>	<i>0.33(6)</i>	<i>0.00</i>	<i>0.00</i>	<i>0.762(3)</i>	<i>0.5(2)</i>	<i>0.9</i>	(1)
		0.34(6)	0.00	0.00	0.745(4)	2.4(3)	0.9	
D1	<i>4b</i>	<i>0.58(6)</i>	<i>0.25</i>	<i>0.426(3)</i>	<i>0.259(1)</i>	<i>5.5(2)</i>	<i>0.8</i>	(1)
		0.48(2)	0.25	0.421(4)	0.257(2)	6.3(3)	0.8	
D2	<i>4b</i>	<i>0.42(2)</i>	<i>0.25</i>	<i>0.390(5)</i>	<i>0.744(2)</i>	<i>5.5(2)</i>	<i>0.9</i>	(1)
		0.52(2)	0.25	0.386(4)	0.744(1)	6.3(3)	0.9	

(the z coordinate for Ta1 atom was held invariant in order to define the origin - *a* : see text)

Table 3: Atomic coordinates, B_{iso} and bond valence sums (Σ) for $\text{LiDSrTa}_2\text{O}_7$ from neutron diffraction data (S.G. I4/mmm) at 250°C

	Site	s.o.f.	x	y	z	$B_{\text{eq}} (\text{\AA}^2)$	Σ	(Σ_{exp})
Ta	<i>4e</i>	1	0.00	0.00	0.3873(1)	1.19	5.1	(5)
Sr	<i>2a</i>	1	0.00	0.00	0.00	1.63	2.1	(2)
O1	<i>2b</i>	1	0.00	0.00	0.50	2.36	1.8	(2)
O2	<i>4e</i>	1	0.00	0.00	0.2862(1)	2.58	(a)	(2)
O3	<i>8g</i>	1	0.00	0.50	0.1022(1)	2.07	2.1	(2)
Li	<i>4d</i>	0.5	0.00	0.50	0.25	3.01	0.8	(1)
D	<i>16m</i>	0.125	0.649(1)	0.649(1)	0.2422(5)	6.59	0.8	(1)

Anisotropic thermal parameters $U_{ij} (\times 10^4)$

	11	22	33	12	13	23
Ta	152(4)	152(4)	12(1)	0(0)	0(0)	0(0)
Sr	223(6)	223(6)	15(1)	0(0)	0(0)	0(0)
O1	339(7)	339(7)	21(1)	0(0)	0(0)	0(0)
O2	476(7)	476(7)	13(1)	0(0)	0(0)	0(0)
O3	142(6)	301(6)	25(1)	0(0)	0(0)	0(0)
Li	459(36)	459(36)	24(4)	0(0)	0(0)	0(0)
D	966(40)	966(40)	55(4)	-116(40)	-45(9)	-45(9)

Table 4: Selected interatomic distances (Å) for $\text{LiDSrTa}_2\text{O}_7$ from neutron diffraction data.

RT

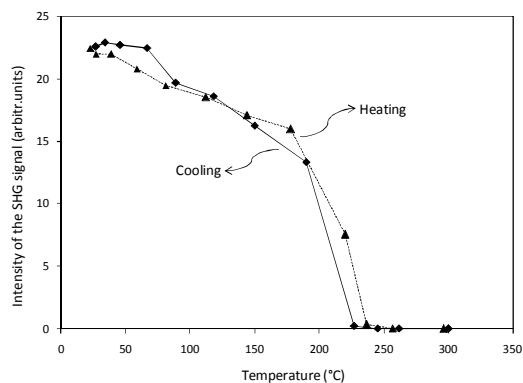
Ta octahedra	Sr polyhedra	Li tetrahedra	D polyhedra
Ta1-O4 : 2×1.938(5)	Sr-O1 : 1×2.590(9)	Li1-O2 : 2×2.09(1)	D1-O2 : 1.95(2)
Ta1-O1 : 1×1.944(8)	Sr-O7 : 2×2.626(7)	Li1-O3 : 2×2.190(9)	D1-O3 : 1.04(2)
Ta1-O6 : 2×1.995(5)	Sr-O5 : 2×2.624(7)	<Li1-O> = 2.14 Å	
Ta1-O2 : 1×2.048(6)	Sr-O1 : 2×2.785(1)		D2-O2 : 0.86(3)
<Ta1-O> = 1.976 Å	Sr-O6 : 2×2.783(7)		D2-O3 : 2.39(3)
	Sr-O1 : 1×2.952(9)	Li2-O2 : 2×2.00(1)	
Ta2-O3 : 1×1.729(8)	Sr-O4 : 2×2.982(8)	Li2-O3 : 2×2.13(3)	
Ta2-O7 : 2×1.983(5)	<Sr-O> = 2.762 Å	<Li2-O> = 2.06 Å	
Ta2-O5 : 2×1.993(5)			
Ta2-O1 : 1×2.297(8)		Li2-O4 : 1×2.22(6)	
<Ta2-O> = 1.996 Å			

160°C

Ta octahedra	Sr polyhedra	Li tetrahedra	D polyhedra
Ta1-O4 : 2×1.947(5)	Sr-O1 : 1×2.63(1)	Li1-O2 : 2×2.09(1)	D1-O2 : 1.96(3)
Ta1-O1 : 1×1.931(8)	Sr-O7 : 2×2.617(7)	Li1-O3 : 2×2.18(1)	D1-O3 : 1.05(3)
Ta1-O6 : 2×1.989(5)	Sr-O5 : 2×2.633(7)	<Li1-O> = 2.14 Å	
Ta1-O2 : 1×2.018(8)	Sr-O1 : 2×2.789(1)		D2-O2 : 0.87(2)
<Ta1-O> = 1.970 Å	Sr-O6 : 2×2.791(8)		D2-O3 : 2.38(2)
	Sr-O1 : 1×2.93(1)	Li2-O2 : 2×2.02(2)	
Ta2-O3 : 1×1.754(8)	Sr-O4 : 2×2.998(8)	Li2-O3 : 2×2.06(3)	
Ta2-O7 : 2×1.993(5)	<Sr-O> = 2.767 Å	<Li2-O> = 2.04 Å	
Ta2-O5 : 2×1.991(5)			
Ta2-O1 : 1×2.326(8)		Li2-O4 : 1×2.36(8)	
<Ta2-O> = 2.008 Å			

250°C

Ta octahedra	Sr polyhedra	Li tetrahedra	D polyhedra
Ta-O2 : 1.897(2)	Sr-O3 : 8×2.746(1)	Li-O2 : 4×2.079(1)	D-O2 : 2.116(6)
Ta-O3 : 4×1.975(1)	Sr-O1 : 4×2.778(1)	<Li1-O> = 2.079 Å	D-O2 : 0.986(7)
Ta-O1 : 1×2.117(1)	<Sr-O> = 2.757 Å		
<Ta1-O> = 1.985 Å			



The layered RP perovskite $\text{LiHSrTa}_2\text{O}_7$ undergoes a reversible structural transition from an orthorhombic to a tetragonal symmetry around 200°C . This transition, from acentric to centric space group, is revealed by the progressive vanishing of the SHG signal as well as thermal diffraction (RX and neutron) and Raman spectroscopy.